International Journal of Biological Macromolecules 300 (2025) 140310

Contents lists available at ScienceDirect

International Journal of Biological Macromolecules

journal homepage: www.elsevier.com/locate/ijbiomac

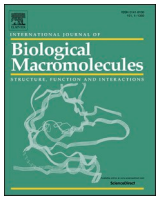

HDAC3 and Snail2 complex promotes melanoma metastasis by epigenetic repression of IGFBP3

Nan Wu [a,b], Qian Sun [a], Liehao Yang [a], Hongyan Sun [a], Zilong Zhou [a], Qianying Hu [a], Chunyi Li [c], Dongxu Wang [c], Ling Zhang [d], Yue Hu [a,*], Xianling Cong [a,*]

[a] Department of Biobank, China-Japan Union Hospital of Jilin University, Changchun 130033, China
[b] Phase I Clinical Trial Research Laboratory, China-Japan Union Hospital of Jilin University, Changchun 130033, China
[c] Institute of Antler Science and Product Technology, Changchun Sci-Tech University, Changchun 130033, China
[d] Key Laboratory of Pathobiology, Ministry of Education, and Department of Biomedical Science, College of Basic Medical Sciences, Jilin University, Changchun 130021, China

ARTICLE INFO

Keywords:
Melanoma
Snail2
EMT
Metastasis

ABSTRACT

The treatment of metastatic melanoma has long posed a complex challenge within clinical practice. Previous studies have found that EMT transcription factors are essential in the development of various cancers through their induction of EMT. Here, we demonstrate that Snail2 expression is dramatically increased in melanoma and is associated with an adverse prognosis. Elevated Snail2 in melanoma cells enhanced migratory and invasive capabilities *in vitro* and *in vivo*. Furthermore, RNA-Seq analysis revealed a significant reduction of IGFBP3 expression in melanoma cells overexpressing Snail2. IGFBP3 might mitigate the Snail2's ability to promote melanoma metastasis *via* the PI3K-AKT pathway. Moreover, Snail2 and HDAC3 collaborate to suppress IGFBP3 transcription through H3K4 deacetylation and H4K5 delactylation. Additionally, the combination of HDAC3 and p-GSK-3β inhibitors significantly improved the treatment outcomes for lung metastasis in melanoma *in vivo*. The results of our study indicate that Snail2, HDAC3, and IGFBP3 play significant roles in melanoma progression and represent promising therapeutic targets.

1. Introduction

Melanoma skin cancer can metastasize in various organs and has a high mortality rate [1]. Despite significant advancements in therapeutic choices, the global incidence and mortality associated with melanoma remain elevated [2]. Regrettably, the 5-year survival rate following melanoma metastasis remains a mere 3–5 % [3–5]. The correlation between metastatic disease and a poor prognosis is well-established [6]. Therefore, it warrants further investigations to elucidate the molecular mechanisms behind melanoma metastasis to enhance the relative survival rate and prognosis [7].

A series of transcriptional repressors regulate tumor metastasis. Snail2 is a transcription factor with a zinc-finger motif that regulates the epithelial-mesenchymal transition (EMT) process during embryogenesis and tumor metastasis [8,9]. The Snail2 protein has been observed to conventionally inhibit the manifestation of E-cadherin in several types of cancer, facilitating the spread and infiltration of tumors, including lung, liver, and colorectal cancer [10,11]. In addition, it has been observed that Snail2 can interact with the promoter of Solute Carrier Family 7 Member 11 (SLC7A11), therefore facilitating the process of ferroptosis in the ovarian cancer cell line, which in turn results in increased ovarian cancer cell migration, proliferation, and invasion [12]. Snail2 facilitates the progression of tumor resistance in non-small cell carcinoma by augmentation of Multidrug resistance-associated protein 2 (MRP2) expression and activity [13]. However, the precise role and pathway underlying Snail2 in melanoma remain unknown.

The incidence and progression of cancers are intricately linked to epigenetic modifications [14]. They primarily influence cancer progression by controlling gene function and expression levels *via* processes such as histone modification, DNA methylation, chromatin structure remodeling, and non-coding RNA regulation [15,16]. Histone modification is a crucial mechanism for the control of chromatin structure remodeling [17,18]. Histone modification encompasses several enzymatic techniques that alter histone proteins, including but not limited to methylation, acetylation, phosphorylation and lactylation. These changes significantly regulate critical biological processes such as

* Corresponding authors at: Department of Biobank, China-Japan Union Hospital of Jilin University, Changchun 130033, China.
E-mail addresses: yuehu@jlu.edu.cn (Y. Hu), congxl@jlu.edu.cn (X. Cong).

https://doi.org/10.1016/j.ijbiomac.2025.140310
Received 11 September 2024; Received in revised form 9 January 2025; Accepted 23 January 2025
Available online 27 January 2025

cancer initiation, metastasis, aging, and metabolism [19]. Histone acetylation is commonly linked to the activation of genes, whereas histone deacetylation, facilitated by HDACs, may contribute to chromatin condensation and a reduction in gene expression [20]. HBO1 has been observed to facilitate tumor development in non-small cell lung cancer by initiating histone acetylation [21]. The deacetylation of TGF-β-activated TAK1, which is reliant on HDAC6, leads to an increase in the release of sIL-6R and facilitates the polarization of macrophages towards the M2 phenotype in colon cancer [22]. The involvement of TRIM21 in the ubiquitination of glutaminase (GAC) through lysine-63 (K63)-linkage after GAC acetylation by HDAC4 has been seen in the process of carcinogenesis in non-small cell lung cancer [23]. As a novel modification, histone lactylation was found by Zhao. in 2019. Research findings suggest that during the final stage of M1 macrophage polarization, histone lactylation is upregulated, which activates specific genes associated with wound healing [24].

This lactate-derived lactylation of histone lysine residues acts as an epigenetic modification, directly facilitating the transcription of genes from chromatin [24]. Lactate is a significant chemical that enhances the up-regulation of cardiac EMT after myocardial infarction *via* the induction of Snail1 lactylation [25]. Elevated levels of histone lactylate in ocular melanoma promote the expression of YTHDF2, thereby recognizing and degrading m^6A-modified PER1 and TP53 mRNA, leading to the malignant progression of ocular melanoma [26]. The process of histone lactylation is mediated by regulatory enzymes rather than occurring spontaneously. It has been observed that HDAC1–3 are effective histone delactylases capable of inducing histone delactylation [27]. However, the substrate and locations in cancer cells are poorly understood.

This work intends to examine the elevated expression of Snail2 and its considerable relationship with poor prognosis of melanoma. Following the manipulation of Snail2 expression by overexpression or knockdown in melanoma cells, a notable alteration in these cells' migratory and invasive capabilities is observed *in vitro* and *in vivo*. Facilitated melanoma metastasis was facilitated by Snail2 through inhibiting IGFBP3 and regulating the PI3K/AKT/GSK3β pathway. Furthermore, our findings indicate that Snail2 interacted with HDAC3 to repress IGFBP3 transcription by deacetylating H3K4 and delactylating H4K5 at the IGFBP3 promoter region. Based on these insights, the combination of HDAC3 with p-GSK-3β inhibitor had more effective inhibitory impact on the lung metastasis of melanoma cells *in vivo*. Therefore, the present findings provide a potential treatment strategy for melanoma therapy.

2. Methods

2.1. Human tissue samples

The study was approved by the Ethics Committee of the China-Japan Union Hospital of Jilin University (2023121303). The Biobank of the China-Japan Union Hospital of Jilin University provided the all-tissue samples for malignant melanoma. These tissue samples were acquired through surgical resections performed on outpatients and inpatients. Liquid nitrogen was used to cryopreserve these tissues. Later, the tissues were kept at −80 °C. Additionally, before undergoing resection surgery, all patients gave informed consent.

2.2. Cell culture

All cell lines were maintained in DMEM (Gibco, USA) with 10 % FBS (Gibco, USA) and incubated at 37 °C with 5 % CO_2. The human melanoma cell lines A375, A2058, and MeWo, the human melanocyte line HEMa, and the human embryonic kidney cell line 293 T were procured from ATCC (USA). The human melanoma cell lines A875 and MV3 were acquired from Shanghai Baiye Biological Company (China). All cell lines used the short tandem repeat (STR) method and were free of mycoplasma contamination. The HDAC3 inhibitors RGFP966 (S7229, Selleckt, USA), GSK3β inhibitors AR-A014418 (S7435, Selleck, USA), and AKT inhibitors Tricribine (S1117, Selleck, USA) were treated in melanoma cells.

2.3. RNA Interference, lentivirus infection and plasmid transfection in vitro

In a 6-well plate, the cells were seeded and allowed to become 60 % confluent. The siRNA (Gene Pharma, China) or plasmid was transfected with Lipo3000 Transfection Reagent (Invitrogen, USA). The subsequent experiments were performed 48 h later. Lentiviral vectors containing green fluorescent protein and either Snail2 or sh-Snail2 and control lentiviral vectors were purchased from Hanbio (China) at a multiplicity of infection (MOI) of 10. The sh-RNA1 (Snail2) sequence was 5′-CCCATTCTGATGTAAAGAAAT-3′ and the sequence of sh-RNA2 (Snail2) was 5′-GATGCATATTCGGACCCACACATTA-3′. Cells infected with lentivirus were screened to identify stable cell lines resistant to puromycin (MCE, USA).

2.4. Real-time quantitative PCR (qPCR)

The Trizol reagent (Invitrogen, USA) was utilized to extract total RNA from cells or tissues, followed by cDNA synthesis using the PrimeScript™ RT reagent Kit purchased from Takara and using 500 ng of total RNA. The experimental procedure involved the use of quantitative real-time PCR (qPCR) reactions utilizing the StepOnePlus Real-time equipment manufactured by Applied Biosystems. The TB Green Premix Ex Taq II (Takara, Japan) was used in experiments. The results were shown as linearized Ct values, and the normalization of target gene mRNA expression levels in relation to GAPDH protein was accomplished using the $2^{-\Delta\Delta Ct}$ approach. Table S3 shows the primers used in this study. All experiments were conducted in triplicate.

2.5. Western blot

The treated cells were rinsed with PBS, detached from the culture dish using a scraper, and collected. The method was conducted under cold conditions, and the whole protein content was recovered from the cells using a radioimmunoprecipitation assay (RIPA; Beyotime, China) lysis buffer supplemented with protease inhibitors (Beyotime, China). The protein concentration was determined using the bicinchoninic acid (BCA) Protein Assay Kit (Beyotime, China). Afterward, the proteins were separated using SDS-PAGE and subsequently deposited onto PVDF membranes manufactured by Millipore (USA). After blocking, the primary antibodies were added and incubated overnight at 4 °C. The antibodies used for Western blotting were as follows: Snail2 (Proteintech #12129–1-AP, 1:1000), GAPDH (Proteintech #5174, 1:1000), E-cadherin (Proteintech #874–1-AP, 1:1000), Fibronectin (Proteintech #15613–1-AP, 1:1000), Vimentin (Proteintech #10366–1-AP, 1:1000), IGFBP3 (Proteintech #10189–2-AP, 1:1000), HDAC1 (Proteintech #10197–1-AP, 1:1000), HDAC2 (Proteintech #12922–1-AP, 1:1000), HDAC3 (Proteintech #10255–1-AP, 1:1000), GSK-3β (CST #12456 T, 1:1000), p-GSK-3β-Tyr216 (Abcam #ab75745, 1:1000), AKT (KleanAB # P290056, 1:1000), p-AKT-Ser473 (Proteintech #28731–1-AP, 1:1000), mTOR (CST #2983, 1:1000), and p-mTOR-Ser2448 (CST #5536, 1:1000). HRP labeled goat anti rabbit secondary antibody (1:5000; abs20040) was purchased from Absin. On the following day, at room temperature, the membranes were subjected to incubation with secondary antibodies labeled with HRP. Subsequently, the immunoreactive bands were observed *via* chemiluminescence.

2.6. CCK-8 assay

The cells that underwent treatment were added onto a 96-well plate, with each containing 3000 cells per 100 μL of volume. A 10 μL solution

of CCK-8 (Beyotime, China) was introduced at 24-h intervals throughout 96 h. The measurement was taken at a wavelength of 450 nm. Afterward, a proliferation curve was constructed, with the optical density (OD) value shown on the y-axis and time represented on the x-axis.

2.7. Migration assays

The migratory capacity of the cells was assessed *via* wound healing assay. In a 12-well plate, the treated MeWo and A375 cells were grown and allowed to reach 100 % confluence. The wound was induced by scratching with a 200 μL sterile pipette tip. The induced lesion was washed with PBS, and DMEM (2 % FBS) was added. The wound margins were then photographed at the initial time point (0 h) and 48 h. The cell migration rates were subsequently assessed to measure the cells' ability to migrate.

2.8. Transwell assay

Cell migration was evaluated in the absence of matrigel, whereas the invasion experiment was conducted using Matrigel (BD, 354235) in transwell chambers (Corning, 8.0 μm). The A375 and MeWo cells were cultured into the top chamber of the transwell where serum-free media (100 μL) was added. Simultaneously, the bottom chamber was filled with 600 μL of DMEM supplemented with 20 % FBS. Following a culture period of 24 to 48 h, the upper chamber was separated and treated with methanol for 15 min using a crystal violet solution (0.1 %). Afterward, the upper chamber was rinsed with PBS. Following that, four sections were chosen at random inside each chamber and then examined under a microscope and photographed using an Olympus IX-53 microscope.

2.9. RNA-Seq and bioinformatics analysis

The RNA samples derived from the cells were subjected to sequencing using an Illumina system performed by Personalbio Biotechnology (China). The acquired reads were then aligned to the GRCh37 human reference genome. The R (edgeR) statistical software tool was utilized for the empirical analysis of digital gene expression to examine differential expression. The analysis involved assessing genes with a fold change >1.5 or < -1.5, a false discovery rate (FDR) < 0.05, and the enrichment of Gene Ontology and Pathway using the R package goProfiles (v3.6). Significant changes were set to a defined threshold: a q-value of 0.05 or lower and an absolute value of $|\log2$ FC (Fold Change) $| = 1.5$ or higher. Differentially expressed mRNAs were selected based on criteria such as FC > 1.5 or FC < 0.68 and $p < 0.05$ by edgeR or DESeq2. The Kyoto Encyclopedia of Genes and Genomes (KEGG), Gene Ontology (GO), and Gene Set Enrichment Analysis (GSEA) were used to enrich the differentially expressed genes (DEGs). The study utilized the Cancer Genome Atlas (TCGA; https://portal.gdc.cancer.gov/) [28], the Gene Expression Profiling Interactive Analysis 2 (GEPIA2; http://gepia2.cancer-pku.cn/#index) [29], and the R language analysis program (https://www.r-project.org/) [30].

2.10. Co-immunoprecipitation (Co-IP)

The cells that had undergone pretreatment were lysed using 300 μL of RIPA lysis buffer (Beyotime, China) supplemented with protease inhibitors. The input sample was identified as having 10 % lysis. The remaining sample was incubated at 4 °C overnight with Anti-Snail2 antibodies and Protein G-Agarose (Roche, Switzerland). The proteins that might be involved in the interaction with Snail2 were further examined using Western blotting.

2.11. Chromatin immunoprecipitation (ChIP) assay

Following the manufacturer's instructions, the experiment was executed *via* the ChIP test kit (Merck, Germany). The immunoprecipitation procedure utilized 1×10^7 cells. Chromatin fragmentation was accomplished by subjecting cell lysates to sonication and then performing immunoprecipitation using antibodies at 4 °C overnight. The DNA precipitates underwent purification and were subsequently identified by qRT-PCR. Histone H3 acetyl K4 antibody from Abcam (ab176799, 5 μg/ChIP, US) and Histone H4 lactyl K5 antibody from PTM-Biolab (PTM-1407RM, 5 μg/ChIP, China) were used. Rabbit IgG from Proteintech (30000–0-AP, China) was introduced into the experimental setup as a negative control for the ChIP reaction and to aid in the normalization procedure. The primers of IGFBP3 promoter were: Forward: 5′-ACACCTTGGTTCTTGTAGA-3′; Reverse: 5′-TGCTTCGCCCTGAGCAGCC-3′.

2.12. Luciferase reporter gene assay

The luciferase reporter assay was conducted as per the guidelines outlined by the Dual-Luciferase Reporter Assay System (Promega, USA). The JASPAR website (http://jaspar.genereg.net/) was accessed to predict the probable binding locations for Snail2 and the IGFBP3 promoter [31]. Subsequently, the promoter of IGFBP3 in the plasmid was constructed (Comate Bioscience, China). Renilla plasmid, Snail2 plasmid, and IGFBP3 promoter plasmid co-transfection were performed in 293 T and A375 cells. The fluorescence measurements of each cellular group were acquired utilizing a microplate reader (TECAN, Infinite M Plex, Switzerland). The obtained results were normalized using the Renilla luciferase fluorescence value.

2.13. Animal models

The animal investigations in the present research were conducted following the guidelines outlined in the Guide for the Care and Use of Laboratory Animals [32]. The Animal Ethics Committee of Changchun Sci-Tech University also examined and approved all experimental procedures and techniques (Approval No. CKARI202308).

2.14. Xenograft tumor model

Female BALB/c nude mice (Charles River, China), aged 5–6 weeks, were randomly allocated into two groups. The investigator was blinded to the group allocation of the mice during the experiment. The experimental procedure involved the subcutaneous injection of cell lines overexpressing Snail2 and control cell lines containing the green fluorescent protein (GFP) into the dorsal region of mice. Each animal received an injection volume of 5×10^6/100 μL. Measurements of body weight and tumor volume in mice were taken at regular 3-day intervals. The tumor volume was determined using the formula: (length $\times$ width^2) / 2. After 30 days, a subset of mice was euthanized and tumor tissue was extracted, weighed, photographed, and split into two equal portions. No animals were excluded from the analysis. The specimen was treated with a 4 % paraformaldehyde solution to facilitate hematoxylin and eosin (H&E) staining and immunohistochemical (IHC) analysis. The remaining portion was later kept at −80 °C for conducting additional experiments.

2.15. Metastasis model

Female BALB/c nude mice (Charles River, China), aged 5–6 weeks were randomly allocated into four groups. The investigator was blinded to the group allocation of the mice during the experiment. Metastasis models were generated by intravenously injecting mice with cell lines that either had an increased expression or reduced expression of Snail2, in addition to control cell lines. These cell lines were also tagged with GFP. Each mouse received an injection of 2×10^6 cells / 100 μL. The growth and condition of the mice were monitored every 3 days. AR-A014418 was dissolved in 5 % DMSO, 40 % PEG300, 5 % Tween-80 and 50 % double-distilled water (ddH_2O). RGFP966 was dissolved in

8 % DMSO, 40 % PEG300, 5 % Tween-80 and 47 % ddH_2O. AR-A014418 (4 mg/kg), RGFP966 (40 mg/kg), or solvent control (Vector) was injected intraperitoneally three times a week. The mice were examined for lung metastasis using an animal *in vivo* imaging system (Tanon, ABL X5pro, China) after 5 weeks. Following this, the mice were sacrificed and examined for lung metastases using H&E staining. No animals were excluded from the analysis.

2.16. Statistical analysis

The statistical analyses were performed using GraphPad Prism 8.0.2 software. The measurements were presented as the mean ± standard deviation (SD) of individual tests performed in triplicate. The unpaired *t*-test was utilized to evaluate the significant difference between the two groups. A p value <0.05 was considered statistical significance. The significance levels used are * $p < 0.05$, ** $p < 0.01$, *** $p < 0.001$, and **** $p < 0.0001$.

3. Results

3.1. High expression levels of Snail2 are associated with poor prognosis in melanoma

EMT transcription factors (EMT-TFs) are closely related to cancer metastasis [33]. In the study, the TCGA database [28] was first used to analyze the correlation between EMT-TFs and the prognostic outcomes of melanoma patients. It was intended to identify pivotal EMT-TFs associated with melanoma metastasis (Fig. 1A-F). A positive correlation between Snail2 expression and melanoma prognosis was observed (Fig. 1B). Additionally, a significant correlation was noted between Snail2 expression level, the degree of melanoma metastasis, and clinical stage (Fig. 1G, Table S1). However, Snail2 expression was not correlated

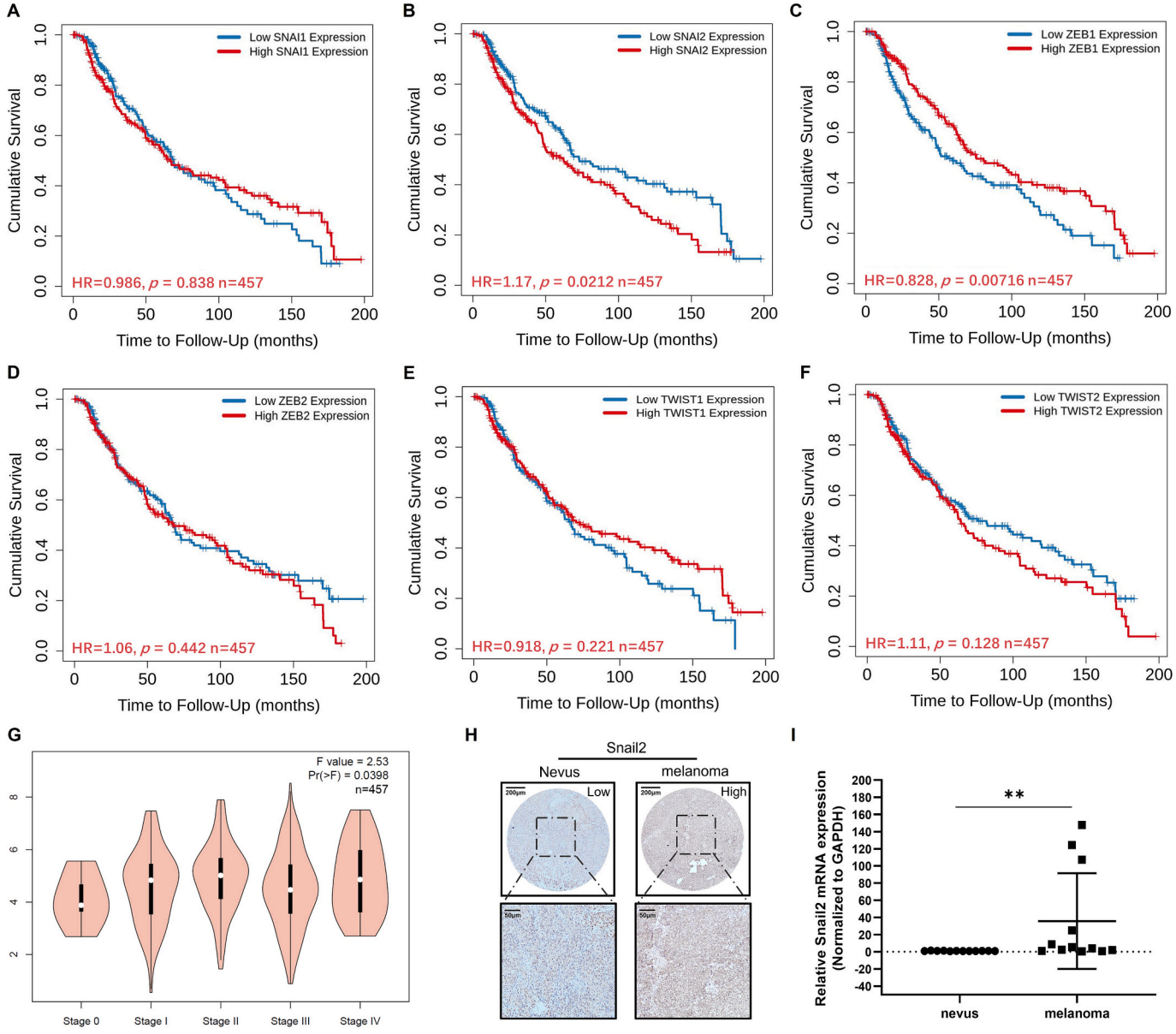

Fig. 1. The expression of EMT-TFs in patients were positively correlated with melanoma and negatively correlated with prognosis. A-F The correlation between EMT-TFs and the prognosis of melanoma patients was analyzed based on TCGA data, $n = 457$. G The relationship between the expression level of Snail2 and tumor clinical stage in melanoma patients was predicted based on TCGA data. H The expression level of Snail2 in nevus and melanoma was detected by IHC, $n = 12$. I The mRNA level of Snail2 in pigmented nevus and melanoma tissues were analyzed by qPCR, n = 12. Scale bar, 50 μm and 200 μm (H) Each experiment was repeated at least three times, data are presented as mean ± SD. ** $p < 0.01$.

with age, gender, ulceration, Clark level, and Breslow thickness (Table S1). To further validate these findings, Snail2 expression was examined in melanoma tissue samples from the China-Japan Union Hospital of Jilin University. The analysis revealed a significant elevation of Snail2 expression in tumor tissues compared to pigmented nevus (Fig. 1H, I). These findings suggest that Snail2 plays a crucial role in melanoma progression and is significantly associated with poor prognosis.

3.2. *Snail2 promotes migration and invasion of melanoma cells in vitro and in vivo*

To gain further insight into the impact of Snail2 on the characteristics of melanoma cells, initially, we first analyzed Snail2 expression in several melanoma cell lines. According to Fig. 2A and B, Snail2 expression was lowest in A375 cell line and highest in the MeWo cell line. Specifically, A375 cell line was used to construct stable overexpression (OE) cell lines (Vector, OE-Snail2). In contrast, the MeWo cell line was used to generated the knockdown cell lines as named shNC, shSnail2–1, and shSnail2–2 (Fig. S1A—C). As shown in Fig. S1D, neither overexpression nor knockdown of Snail2 significantly altered melanoma cell proliferation ability. To explore the functional role of Snail2 in melanoma metastasis, we assessed melanoma cell invasion and migration abilities using wound healing and Transwell assays. Snail2 overexpression significantly enhanced melanoma cell migration and invasion capabilities (Fig. 2C, D). Conversely, Snail2 knockdown significantly reduced these abilities *in vitro* (Fig. 2E, F).

EMT plays a crucial role in tumor metastasis and is characterized by distinct morphological changes and signature markers [34]. As Fig. S1A shows, A375 OE-Snail2 cells exhibited a larger size, reduced intercellular connections, elongated spindle shapes, and a clear mesenchymal-like morphology. Conversely, MeWo shSnail2 cells displayed smaller sizes, increased intercellular junctions, rounded shapes, and an epithelial-like morphology. These morphological changes suggested that Snail2 might induce EMT in melanoma cells. To confirm this, the EMT markers were examined to determine the promotion of EMT by Snail2. In A375 OE-Snail2 cells, E-cadherin expression was significantly reduced, while mesenchymal markers Vimentin and Fibronectin were significantly increased (Fig. 2G). Conversely, MeWo shSnail2 cells displayed increased E-cadherin levels and decreased Vimentin and Fibronectin expression (Fig. 2H). These findings revealed that Snail2 promotes EMT, enhancing the metastatic potential of melanoma cells *in vitro*.

We further examined the effect of Snail2 on melanoma proliferation and metastasis *in vivo*. Consistent with *in vitro* findings, overexpression of Snail2 did not significantly alter tumor volume, weight, or proliferative ability (Fig. 3 A-F). However, using a lung metastasis model, we observed a significant increase in lung metastases in the OE-Snail2 group, while mice in the shSnail2 group exhibited a significant reduction in lung metastases (Fig. 3 G-J). These results strongly indicate that Snail2 enhances the migration, invasion, and EMT processes in melanoma cells and promotes metastasis both *in vitro* and *in vivo*.

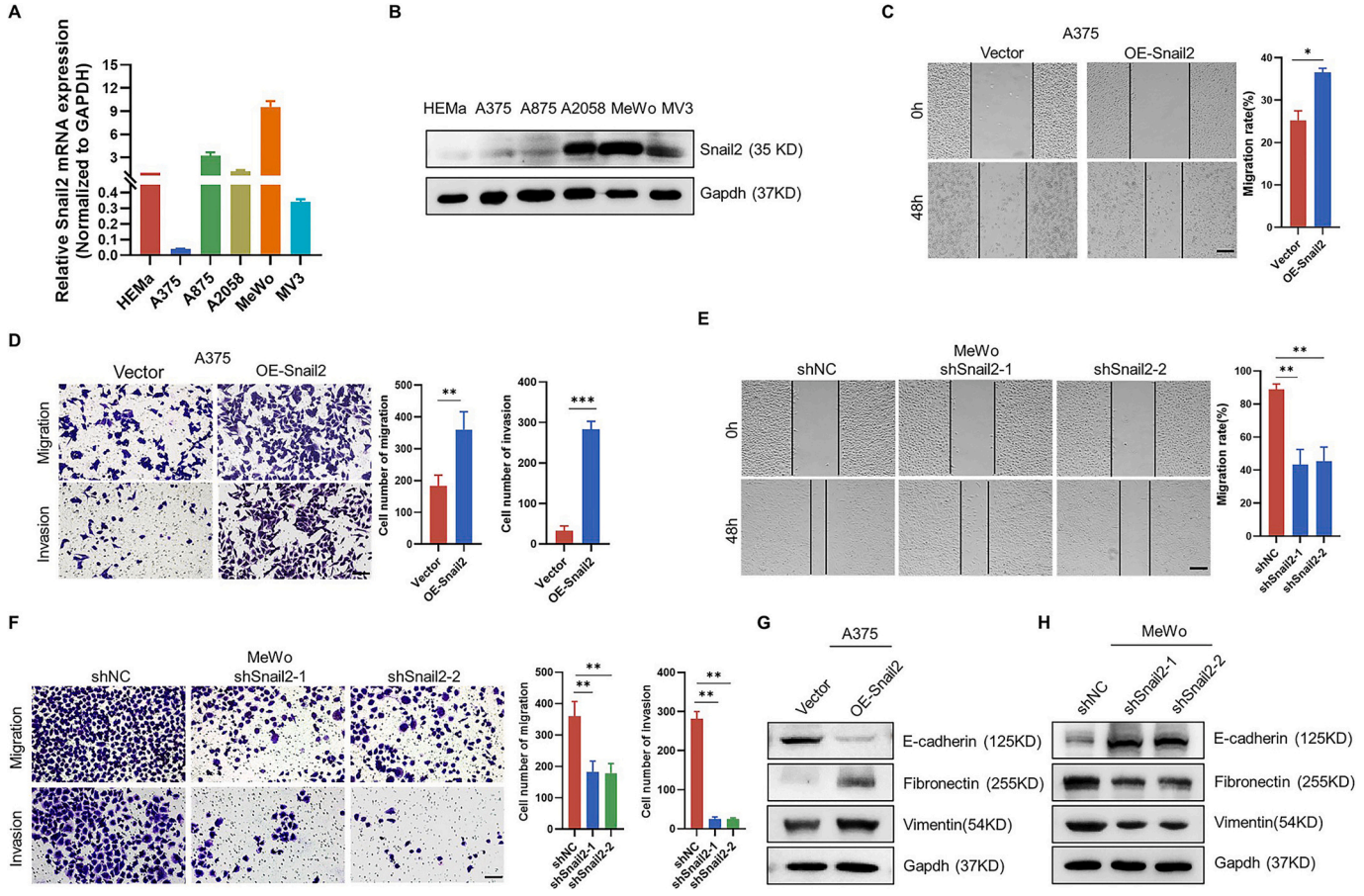

Fig. 2. Snail2 promotes migration, invasion, and EMT in melanoma cells *in vitro*. A, B The mRNA and protein expression level of Snail2 in melanoma cells were detected by qPCR and Western blot. C, E The migration of melanoma cells was detected *via* wound healing assay after over-expressing or silencing Snail2. The statistical differences in the bar graph are shown in the right of the image results. D, F The transwell assay was used to detect the migration and invasion of melanoma cells after over-expressing or silencing Snail2. The statistical differences in the bar graph are shown in the right of the image results. G, H The expression level of EMT markers in melanoma cells was detected *via* Western blot following over-expressing or silencing of Snail2. Scale bar, 200 μm (C, E), 100 μm (D, F). Data are presented as mean ± SD, $n = 3$. * $p < 0.05$, ** $p < 0.01$, *** $p < 0.001$.

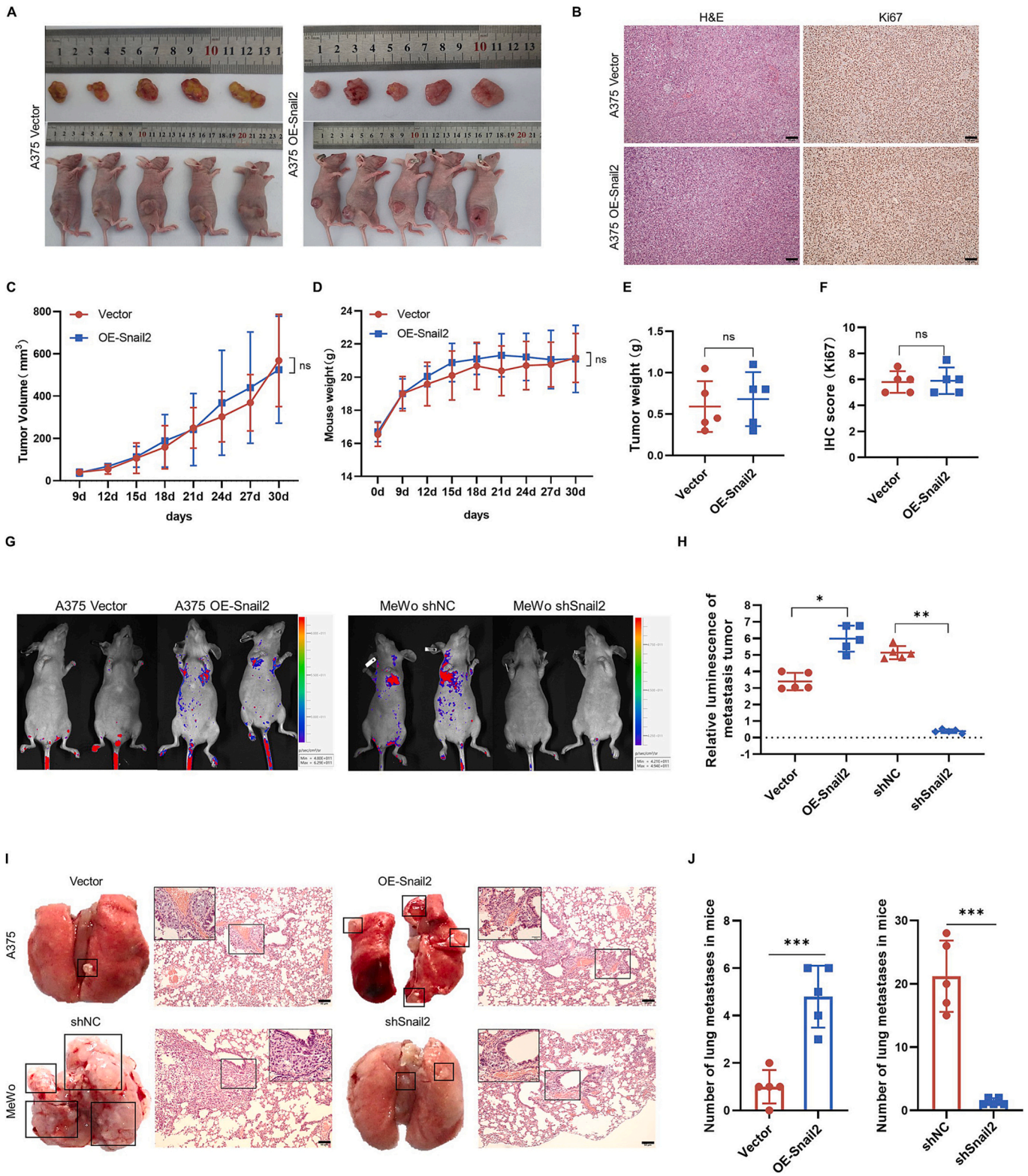

Fig. 3. Snail2 promotes metastasis of melanoma cells *in vivo*. A Xenografts derived from A375 OE-Snail2 and Vector cells in nude mice, $n = 5$ mice/group. B, F Xenografts tumor sections with H&E staining and Ki67 IHC staining. Representative images of H&E (B) and Ki67 IHC (F), $n = 5$. C, D Measurements of tumor volume and mouse weight were taken at 3-day intervals. E Tumor weight was recorded after mice were sacrificed to isolate tumors. G, H The metastasis status of melanoma cells assessed after over-expression or silencing of Snail2 *via* bioluminescence imaging *in vivo*. I, J Representative Photographs of mice lung metastatic nodules and H&E staining after over-expression or silencing of Snail2. Scale bar, 50 μm (B, I). Data are presented as mean ± SD, n = 5. * $p < 0.05$, ** $p < 0.01$, ns, no significance.

3.3. Snail2 mediated the downregulation of IGFBP3

To explore the specific mechanism by which Snail2 promotes melanoma metastasis, we performed RNA-Sequencing (RNA-Seq) on A375 OE-Snail2 and vector cell lines. We conducted an analysis of differentially expressed genes (Fig. 4 A). Subsequently, the findings indicate a potential association between Snail2 and various cellular processes, including cell migration, cell morphology, cell adhesion, the PI3K-Akt signaling pathway, and other biological processes associated with melanoma by GO (Gene Ontology), KEGG (Kyoto Encyclopedia of Genes and Genomes), and GSEA (Gene Set Enrichment Analysis) enrichment analyses (Fig. 4 B, C, and Fig. S2 A). Seven putative target genes that might be associated with the development of tumors were selected and subjected to investigation. We found that the expression of IGFBP3, LAMA4, AK4, LAMA2 and FCGR2A were significantly reduced in A375 OE-Snail2 cell line, but only IGFBP3 expression was significantly increased in MeWo shSnail2 cell lines (Fig. 4 D, E). Furthermore, analysis of the TCGA database revealed a significant negative correlation between Snail2 and IGFBP3 expression in melanoma samples (Fig. 4 F), and the same trend was shown in cell lines by Western blot (Fig. 4 G, H). The above results indicate that Snail2 inhibits the expression of IGFBP3 in melanoma cells.

3.4. Snail2-IGFBP3 promotes metastasis of melanoma cells via the PI3K-Akt pathway

To further investigate the role of IGFBP3 in Snail2-induced melanoma progression, we assessed the migration and invasion abilities of melanoma cells through IGFBP3 overexpression or knockdown experiments. Compared to the control (A375 OE-Snail2), IGFBP3 overexpression significantly reduced the migration and invasion abilities of melanoma cells (Fig. 5 A, B and Fig. S2 B, C). In contrast, IGFBP3 knockdown restored the migratory and invasive capacities of melanoma cells (Fig. 5 C, D). Additionally, following IGFBP3 overexpression, the expression of E-cadherin increased significantly, while the expression of mesenchymal markers Fibronectin and Vimentin decreased (Fig. 5 E). Conversely, IGFBP3 knockdown resulted in the opposite effects, with marked increases in Fibronectin and Vimentin levels and a significant reduction in E-cadherin expression (Fig. 5 F). These findings suggest that Snail2 promotes melanoma cell migration, invasion, and EMT through the suppression of IGFBP3 expression.

The PI3K-Akt pathway is widely recognized as a critical signaling mechanism involved in cell migration, proliferation, and glucose metabolism, all of which contribute to cancer progression [35,36]. KEGG analysis of RNA-seq data suggests that Snail2 may modulate the

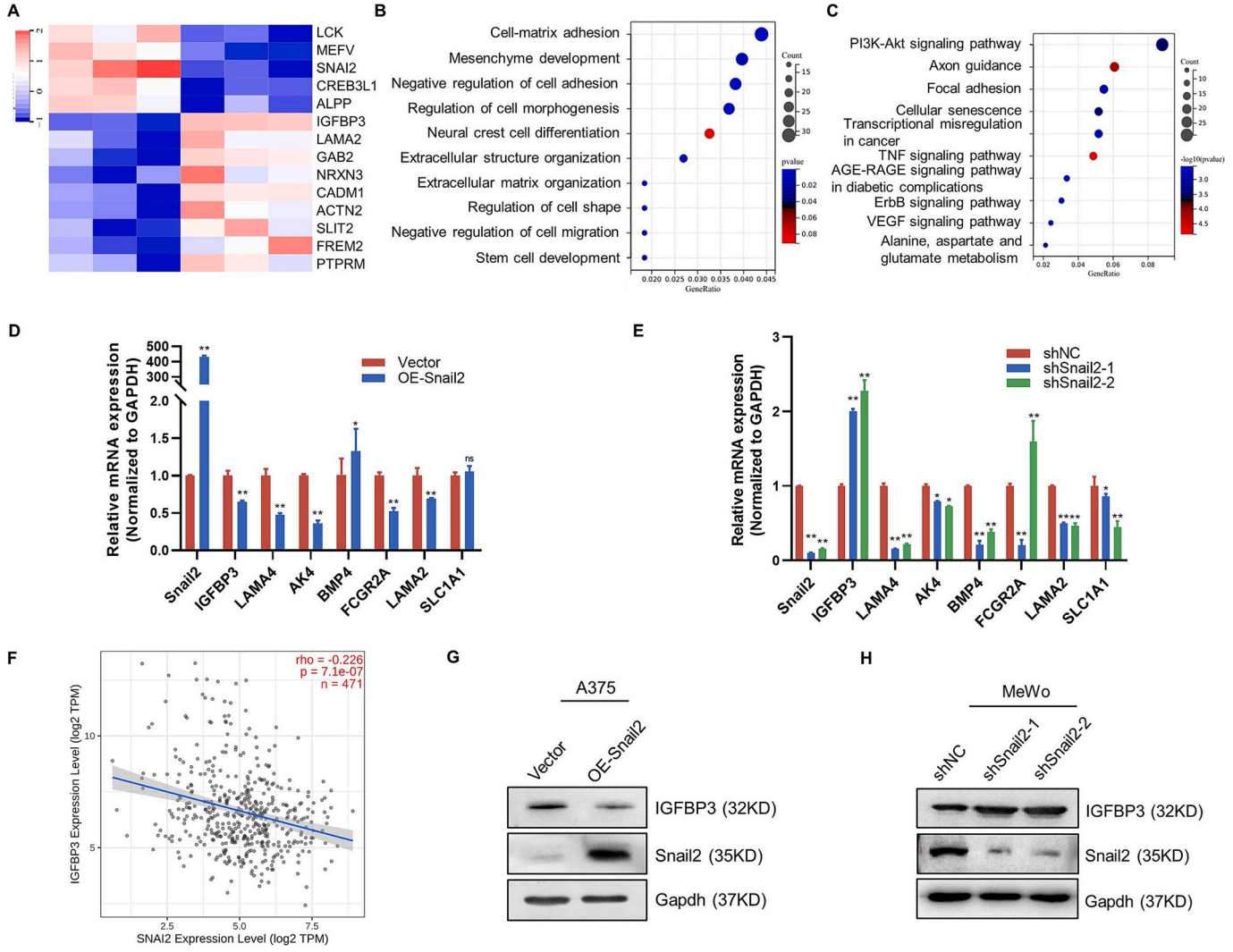

Fig. 4. Snail2 inhibits the expression of IGFBP3 in melanoma cells. A Heat map shows the top 15 DEGs. B The GO and KEGG enrichment analysis. C Gene Set Enrichment Analysis. D, E DEGs in A375 and MeWo were detected using qPCR. F The association between Snail2 and IGFBP3 in melanoma was examined utilizing the TCGA database to get the analysis results, $n = 471$. G, H The expression of IGFBP3 was detected by Western blotting in cell lines following over-expression or silencing of Snail2. Data are presented as mean ± SD, n = 3. * $p < 0.05$, ** $p < 0.01$, ns, no significance.

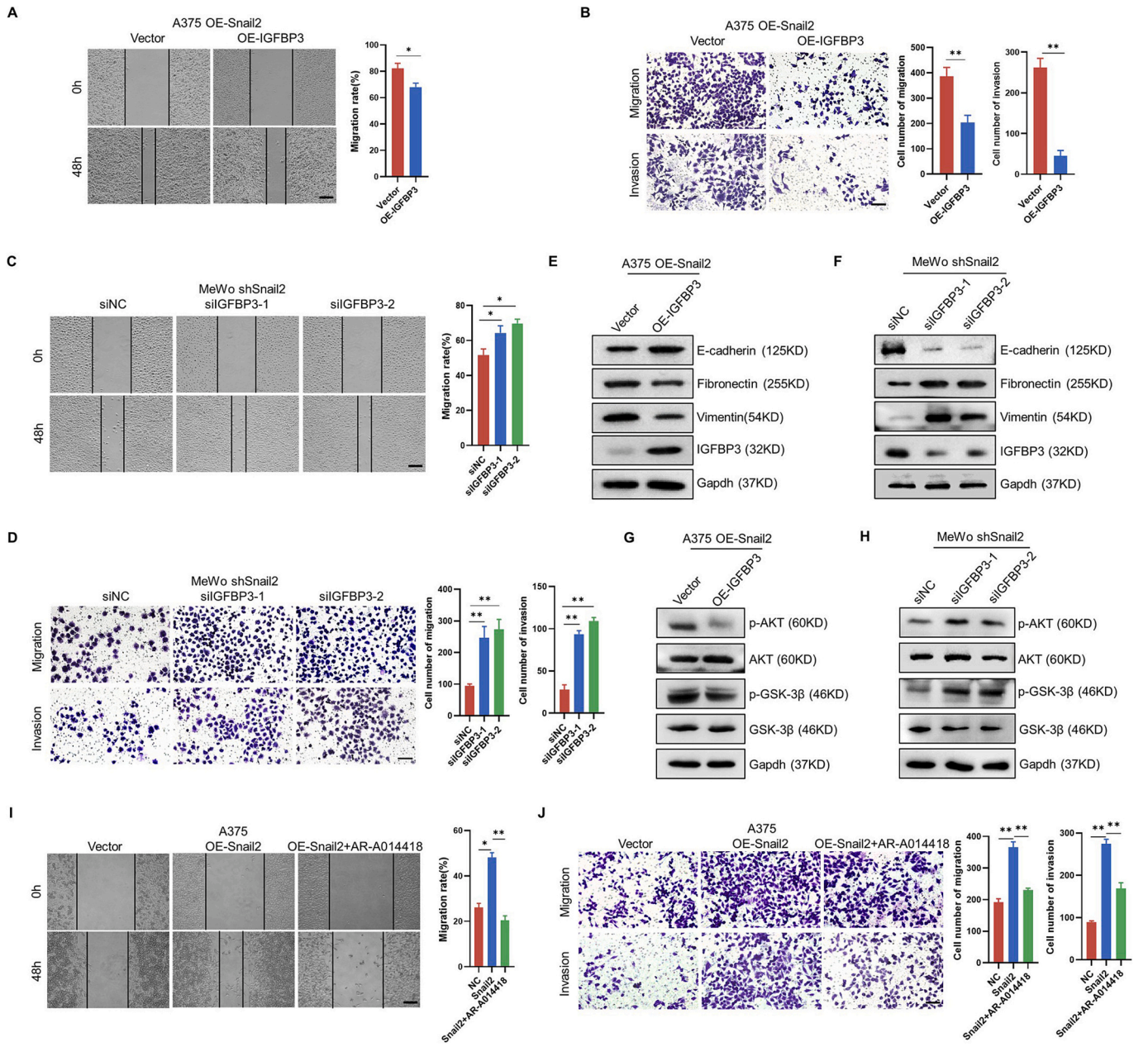

Fig. 5. Snail2 promotes migration and invasion of melanoma cells *via* manipulation of the levels of IGFBP3. A, B The migration of melanoma cells was detected by wound healing assay. The statistical differences in the bar graph are shown in the right of the image results. C, D The migration and invasion of melanoma cells were analyzed by transwell assay. The statistical differences in the bar graph are shown in the right of the image results. E, F The protein levels of EMT markers in melanoma cells were detected using the Western blot. G, H The expression level of the PI3K/AKT pathway was detected *via* Western blot. I The migration of A375 cells was detected by wound healing after over-expression of Snail2 or treatment with AR-A014418. The statistical differences in the bar graph are shown in the right of the image results. J The transwell assay was used to detect the migration and invasion of A375 cells after over-expressing Snail2 or treatment with AR-A01441. The statistical differences in the bar graph are shown in the right of the image results. Scale bar, 200 μm (A, C, I), 100 μm (B, D, J).Data are presented as mean ± SD, n = 3. * $p < 0.05$, ** $p < 0.01$.

PI3K-Akt signaling pathway in melanoma cells. Given Snail2's involvement in melanoma metastasis, both PI3K-Akt-mTOR and PI3K-Akt-GSK3β play essential roles in tumor metastasis [37,38]. Subsequently, we verified the AKT and downstream substrates including mTOR and GSK3β by Western blot. These data indicated that p-AKT and p-GSK3β levels were significantly reduced following IGFBP3 overexpression (Fig. 5 G), whereas IGFBP3 knockdown resulted in a significant increase in p-AKT and p-GSK3β levels (Fig. 5 H). Notably, the expression levels of mTOR and p-mTOR remained unchanged (Fig. S2 D, E). To validate the results, AKT inhibitors (Triciribine) and GSK3β Inhibitor (AR-A014418) were used in malignant melanoma cells (A375) (Fig. S2 F, G). The findings demonstrated that AR-A014418 effectively inhibited the metastatic potential of melanoma cells *in vitro* (Fig. 5 I, J and Fig. S2 H, I). These results collectively suggest that Snail2 promotes melanoma metastasis through the suppression of IGFBP3, leading to the activation of the PI3K-Akt-GSK3β signaling pathway.

3.5. *Snail2 interacts with HDAC3 to repress IGFBP3 transcription through H3K4 deacetylation and H4K5 delactylation*

Our previous study demonstrated that Snail2 can cooperate with histone-modifying enzymes to suppress the transcription of specific

genes [39]. As shown in Fig. 6 A, HDAC1–3 were found to interact with Snail2 in melanoma cells. To further investigate the effect of Snail2 on the transcriptional regulation of IGFBP3, we performed a luciferase reporter assay. Using the JASPAR database, we predicted potential Snail2 binding sites in the promoter region of IGFBP3 (Fig. 6 B and Table S2). We then constructed three plasmids (P1, P2, and P3) containing the firefly luciferase gene (pGL3-IGFBP3-LUC) with the respective binding sites (Fig. 6 C). The co-transfection of plasmids, including promoter, Snail2, and Renilla, was performed on 293 T and A375 cells. Compared to controls, the activities of the IGFBP3 promoters P1, P2, and P3 were significantly suppressed following Snail2 overexpression (Fig. 6 D). To explore the cooperation between Snail2 and HDAC1–3 in repressing

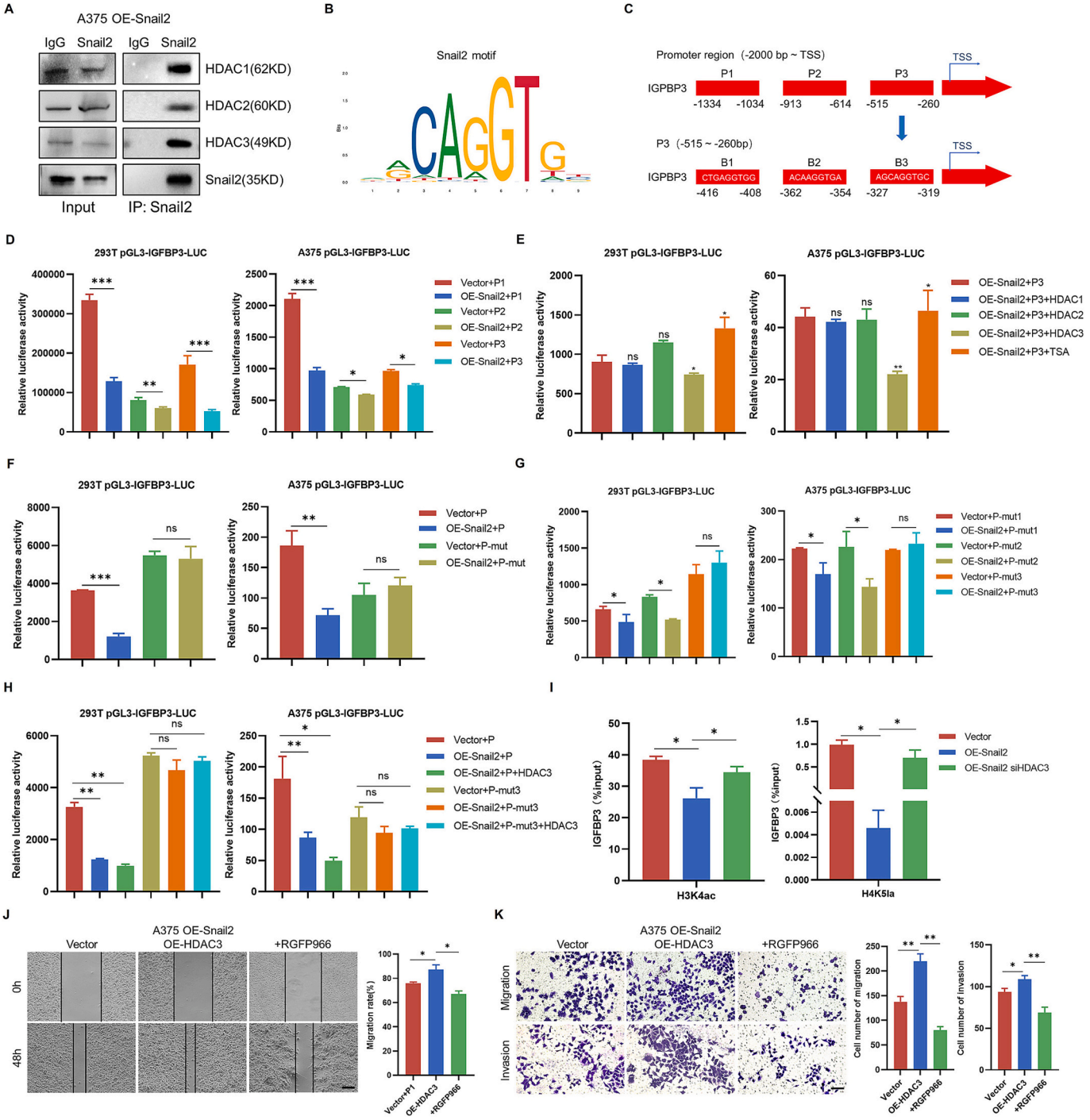

Fig. 6. Snail2 collaborates with HDAC3 to inhibit IGFBP3 transcription through H3K4 deacetylation and H4K5 delactylation. A The interaction between Snail2 and HDAC1–3 in melanoma cells was detected *via* the Co-IP assay. B The motif of Snail2 in the Jaspar database. C The plasmid construction of the IGFBP3 promoter region. D, E The activity of the IGFBP3 promoter was detected *via* the dual luciferase reporter gene assay following overexpression of Snali2 and HDAC1–3. F Construction of the plasmid with a mutation at the binding site in the IGFBP3 promoter. G, H The activity of the mutated IGFBP3 promoter was detected *via* the dual luciferase reporter gene assay following overexpression of Snail2 and HDAC3. I H3K4ac and H4K5la levels in the IGFBP3 promoter region of A375 OE-Snail2 cells were detected *via* ChIP qPCR. J, K The migration and invasion abilities of melanoma cells were analyzed using wound healing and transwell assays after overexpressing HDAC3 and adding the HDAC3 inhibitor (RGFP966). The statistical differences in the bar graph are shown in the right of the image results. Scale bar, 200 μm (J), 100 μm (K).Data are presented as mean ± SD, n = 3. * $p < 0.05$, ** $p < 0.01$, *** $p < 0.001$, ns, no significance.

IGFBP3 transcription, we employed a co-transfection method using HDAC1–3 inhibitors (TSA) and HDAC1–3 plasmids. The results showed no alterations in the transcriptional activity of IGFBP3 promoters P1 and P2 upon HDAC1 or HDAC2 overexpression (Fig. S3 A, B). However, HDAC3 overexpression significantly reduced the transcriptional activity of the P3 region of the IGFBP3 promoter, whereas TSA treatment reversed this suppression, suggesting that Snail2 interacts specifically with HDAC3 to repress IGFBP3 transcription *via* the P3 region (Fig. 6 E). The P3 region contains three putative binding sites (Supplementary materials 1). We constructed the mutant plasmid (P-mut) by simultaneously mutating these three binding sites (Fig. S3 C). The results indicated no statistically significant change in transcriptional activity of P-mut after Snail2 overexpression in 293 T and A375 cells (Fig. 6 F). Additionally, we constructed three mutant plasmids (P-mut1, P-mut2, and P-mut3), each targeting one of the three binding sites (B1, B2, B3) (Fig. 6 G). Compared to the control, transcriptional activities of P-mut1 and P-mut2 were significantly reduced following Snail2 overexpression, while P-mut3 showed no significant change. HDAC3 overexpression had no effect on P-mut3 activity, indicating that Snail2 and HDAC3 repress IGFBP3 transcription through P3 region (Fig. 6 H).

Histone modifications such as H3K4 acetylation (H3K4ac) and H4K5 lactylation (H4K5la) are regulated by HDAC3 [40,41]. The results showed that Snail2 overexpression significantly reduced H3K4ac and H4K5la levels in the IGFBP3 promoter region (Fig. 6 I). Conversely, interfering with HDAC3 activity restored H3K4ac and H4K5la levels in the IGFBP3 promoter, even in the presence of Snail2 overexpression. (Fig. 6 I). These results suggest that Snail2 cooperated with HDAC3 to inhibit IGFBP3 transcription through H3K4 deacetylation and H4K5 delactylation. We further investigated the role of HDAC3 in the melanoma metastasis.

Overexpression of HDAC3 significantly enhanced melanoma cell migration and invasion abilities, while HDAC3 suppression resulted in a significant reduction in these abilities (Fig. 6 J, K). Additionally, HDAC3 overexpression in A375 cells significantly reduced IGFBP3 expression, whereas HDAC3 knockdown in MeWo cells resulted in a marked increase in IGFBP3 expression (Fig. S3 D, F). These findings suggest that Snail2 and HDAC3 cooperate to facilitate melanoma metastasis by repressing IGFBP3 transcription *via* H3K4 deacetylation and H4K5 delactylation.

3.6. Inhibitors of HDAC3 and p-GSK-3β suppress melanoma metastasis in vivo

Melanoma frequently metastasizes to the lungs, posing a significant challenge in clinical treatment [42]. Based on our *in vitro* results, we evaluated the therapeutic potential of combination treatment using HDAC3 inhibitors (RGFP966) and p-GSK-3β inhibitors (AR-A014418) in a lung metastasis model of melanoma cells. As shown in Fig. 7, the combined administration of RGFP966 and AR-A014418 demonstrated a stronger inhibitory effect on melanoma lung metastasis compared to either treatment alone, as evidenced by *in vivo* imaging analysis (Fig. 7 A, B, C and D). Furthermore, immunohistochemical (IHC) staining of clinical melanoma tissue samples was performed to evaluate the expression levels of Snail2, HDAC3, IGFBP3, and phosphorylated GSK-3β (Fig. 7 E). The IHC results revealed positive correlations between Snail2 and HDAC3 expression levels (Fig. 7 F), while both Snail2 and HDAC3 showed negative correlations with IGFBP3 expression (Fig. 7 G, H). Additionally, IGFBP3 expression was inversely correlated with GSK-3β phosphorylation (Fig. 7 I), whereas both Snail2 and HDAC3 exhibited positive correlations with GSK-3β phosphorylation (Fig. 7 J, K). These findings suggest that Snail2 regulates melanoma metastasis by repressing IGFBP3 and modulating the PI3K/AKT/GSK3β signaling pathway.

4. Discussion

Melanoma is notorious for its metastatic behavior and remains one of the most aggressive solid tumors, with metastasis being the primary cause of patient mortality [43–46]. Despite significant progress in understanding melanoma biology, the molecular mechanisms driving metastasis remain incompletely understood. A recent study demonstrated that the Hedgehog/GLI signaling pathway promotes melanoma progression by activating Snail2 transcription [47]. However, the downstream pathways and functional roles of Snail2 in melanoma metastasis remain unclear. In the present study, we identified a significant correlation between elevated Snail2 expression and a poor prognosis in melanoma patients. Moreover, the findings indicated that Snail2 interacts with HDAC3 to repress IGFBP3 transcription by deacetylating H3K4 and delactylating H4K5 at the IGFBP3 promoter region. Indeed, the epigenetic modification suppresses IGFBP3 expression, ultimately facilitating melanoma cell metastasis (Fig. 8). Furthermore, our findings demonstrated that IGFBP3 serves as a critical suppressor of Snail2-mediated metastasis, functioning through the PI3K/Akt/GSK3β signaling pathway. Overexpression of IGFBP3 reversed Snail2-induced metastatic potential by inhibiting p-AKT and p-GSK3β levels, while knockdown of IGFBP3 enhanced melanoma cell migration, invasion, and EMT characteristics. Based on these insights, the combination of HDAC3 inhibitor (RGFP966) and p-GSK3β inhibitor (AR-A014418) exhibited a synergistic therapeutic effect in reducing melanoma lung metastasis *in vivo*. These findings suggest that targeting the Snail2-HDAC3-IGFBP3 axis may represent a novel therapeutic strategy for melanoma treatment.

Histone lysine lactylation has recently emerged as a novel epigenetic modification that directly enhances gene transcription [48–50]. For example, in human hepatocellular carcinoma, royal jelly acid (from honeybees) was shown to regulate lactylation at H3K9la and H3K14la sites, affecting tumor growth *via* glycolytic pathway modulation [51]. Similarly, in clear cell renal cell carcinoma (ccRCC), histone lactylation was linked to tumor progression and poor prognosis [52]. Evidence also suggests that Class I histone deacetylases, notably HDAC1–3, are recognized as histone lysine delactylases, and their enzymatic activity has significant implications in both cancer biology and developmental processes [27]. These findings highlight histone lactylation as a crucial epigenetic regulator with potential therapeutic relevance in oncology [53,54]. Here, we confirm that Snail2 and HDAC3 collaboratively repress IGFBP3 transcription not only through deacetylating H3K4ac but also by delactylating H4K5la. This dual histone modification mechanism provides a deeper understanding of how Snail2 drives melanoma metastasis at the epigenetic level. Moreover, treatment with the HDAC3 inhibitor RGFP966 significantly reversed lung metastasis in melanoma models, reinforcing the therapeutic potential of targeting histone modifications in melanoma. These findings imply that modulating histone lactylation and acetylation may serve as a promising therapeutic avenue for melanoma intervention.

In conclusion, our study uncovered a novel regulatory mechanism involving Snail2, HDAC3, and IGFBP3 in melanoma metastasis, mediated through epigenetic modifications and the PI3K/Akt/GSK3β pathway. These findings provide important mechanistic insights and highlight Snail2, HDAC3, and IGFBP3 as potential therapeutic targets for melanoma treatment. Future research should focus on further exploring the upstream regulation of Snail2 expression and the impact of Snail2 on the tumor microenvironment to fully understand its role in melanoma progression and therapy.

Availability of data and materials

Data are available upon reasonable request.

CRediT authorship contribution statement

Nan Wu: Writing – review & editing, Writing – original draft, Supervision, Methodology, Investigation. **Qian Sun:** Methodology. **Liehao Yang:** Investigation. **Hongyan Sun:** Visualization. **Zilong Zhou:**

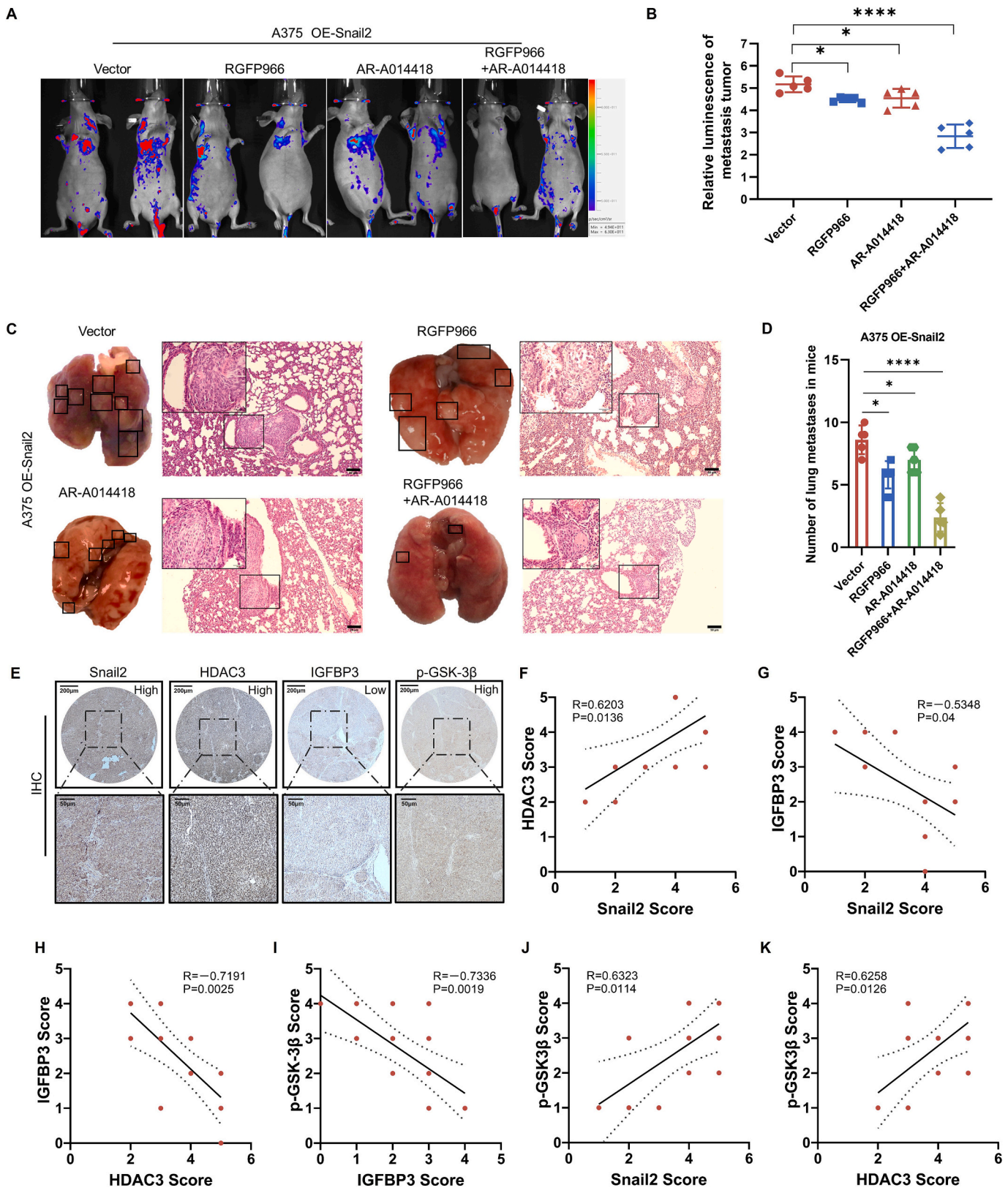

Fig. 7. Anti-metastatic effects of RGFP966 combined with AR-A014418 *in vivo*, and the expression of Snail2, HDAC3, IGFBP3 and p-GSK-3β in melanoma samples from patients. A, B Detection of the metastasis status of melanoma cells *in vivo via* bioluminescence imaging, n = 5. C, D Representative photographs of mice lung metastatic nodules and H&E staining images, n = 5. E —K The expression level of Snail2, HDAC3, IGFBP3 and p-GSK3β were detected *via* IHC, $n = 15$, and measurement of the correlation between Sanil2, HDAC3, IGFBP3 and p-GSK3β was analyzed. Scale bar, 50 μm (C, E) and 200 μm (E). Data are presented as mean ± SD. * $p < 0.05$, **** $p < 0.0001$.

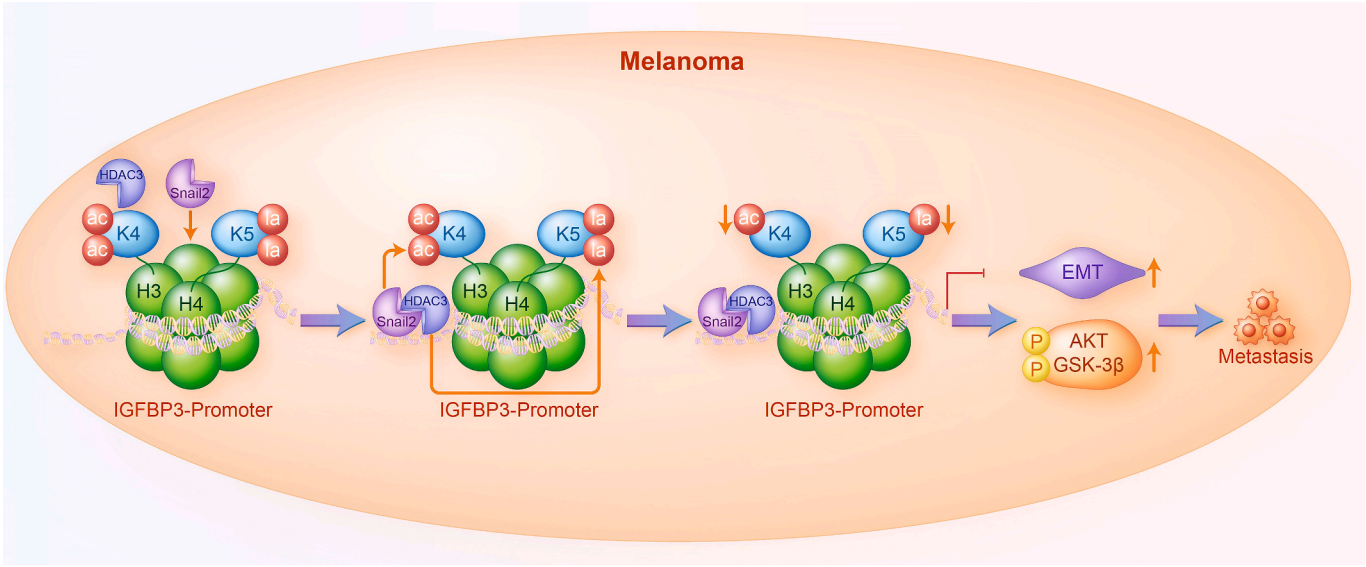

Fig. 8. Pattern diagram for the role of Snail2 in the promotion of metastasis of melanoma.

Visualization. **Qianying Hu:** Supervision. **Chunyi Li:** Visualization. **Dongxu Wang:** Supervision. **Ling Zhang:** Methodology. **Yue Hu:** Conceptualization. **Xianling Cong:** Conceptualization.

Funding

This work was supported by the Scientific and Technology Development Program of Jilin Province (Grant No. YDZJ202501ZYTS730, and YDZJ202501ZYTS133), the Health Talent Project of Jilin Province department of Finance (2024SCZ90), Bethune Project of Jilin University (Grant No.2023B21), China-Japan Union Hospital and College of Basic Medical Sciences, Jilin University Union Project (Grant No. KYXZ2022JC05).

Declaration of competing interest

The authors declare that they have no known competing financial interests or personal relationships that could have appeared to influence the work reported in this paper.

Appendix A. Supplementary data

Supplementary data to this article can be found online at https://doi.org/10.1016/j.ijbiomac.2025.140310.

References

[1] R.L. Siegel, K.D. Miller, H.E. Fuchs, A. Jemal, Cancer statistics, 2022, CA Cancer J. Clin. 72 (2022) 7–33.
[2] Thomson, H. M., Fortin Ensign, S. P., Edmonds, V. S., Sharma, A., Butterfield, R. J., 3rd, Schild, S. E., Ashman, J. B., Zimmerman, R. S., Patel, N. P., Bryce, A. H., Vora, S. A., Sio, T. T., and Porter, A. B. (2023) Clinical outcomes of stereotactic radiosurgery-related radiation necrosis in patients with intracranial metastasis from melanoma. Clinical Medicine Insights. Oncology 17, 11795549231161878.
[3] Li, Z., Fang, Y., Chen, H., Zhang, T., Yin, X., Man, J., Yang, X., and Lu, M. (2022) Spatiotemporal trends of the global burden of melanoma in 204 countries and territories from 1990 to 2019: Results from the 2019 global burden of disease study. Neoplasia (New York, N.Y.) vol. 24, 12–21.
[4] R.L. Siegel, K.D. Miller, N.S. Wagle, A. Jemal, Cancer statistics, 2023, Ca-a Cancer Journal for Clinicians 73 (2023) 17–48.
[5] K.D. Miller, L. Nogueira, T. Devasia, A.B. Mariotto, K.R. Yabroff, A. Jemal, J. Kramer, R.L. Siegel, Cancer treatment and survivorship statistics, 2022, CA Cancer J. Clin. 72 (2022) 409–436.
[6] V.A. Gâta, A. Roman, M. Muntean, D. Morariu, C.I. Vlad, E.A. Bonci, A. Irimie, P. Achimaș-Cadariu, Prognostic factors for in-transit metastasis in patients with malignant melanoma, Medicine and pharmacy reports 95 (2022) 40–46.
[7] Rosen, C., Mayes, T., Overholt, C., and Lucke-Wold, B. (2023) Treatment of melanoma metastasis: surgical, chemotherapy, and innovation. *Med discoveries* **2**.
[8] J.M. Rukstalis, J.F. Habener, Snail2, a mediator of epithelial-mesenchymal transitions, expressed in progenitor cells of the developing endocrine pancreas, Gene expression patterns : GEP 7 (2007) 471–479.
[9] K. Masuo, R. Chen, A. Yogo, A. Sugiyama, A. Fukuda, T. Masui, S. Uemoto, H. Seno, S. Takaishi, SNAIL2 contributes to tumorigenicity and chemotherapy resistance in pancreatic cancer by regulating IGFBP2, Cancer Sci. 112 (2021) 4987–4999.
[10] Y. Hu, M. Dai, Y. Zheng, J. Wu, B. Yu, H. Zhang, W. Kong, H. Wu, X. Yu, Epigenetic suppression of E-cadherin expression by Snail2 during the metastasis of colorectal cancer, Clin. Epigenetics 10 (2018) 154.
[11] Y. Hu, Y. Zheng, M. Dai, X. Wang, J. Wu, B. Yu, H. Zhang, Y. Cui, W. Kong, H. Wu, X. Yu, G9a and histone deacetylases are crucial for Snail2-mediated E-cadherin repression and metastasis in hepatocellular carcinoma, Cancer Sci. 110 (2019) 3442–3452.
[12] Y. Jin, L. Chen, L. Li, G. Huang, H. Huang, C. Tang, SNAI2 promotes the development of ovarian cancer through regulating ferroptosis, Bioengineered 13 (2022) 6451–6463.
[13] X. Zhang, W. Liu, K. Edaki, Y. Nakazawa, S. Takahashi, H. Sunakawa, K. Mizoi, T. Ogihara, Slug mediates MRP2 expression in non-small cell lung Cancer cells, Biomolecules 12 (2022).
[14] Z. Zhao, A. Shilatifard, Epigenetic modifications of histones in cancer, Genome Biol. 20 (2019) 245.
[15] A. Kumar, L. Emdad, P.B. Fisher, S.K. Das, Targeting epigenetic regulation for cancer therapy using small molecule inhibitors, Adv. Cancer Res. 158 (2023) 73–161.
[16] R. Gupta, Epigenetic regulation and targeting of ECM for cancer therapy, Am. J. Physiol. Cell Physiol. 322 (2022) C762–c768.
[17] J.E. Audia, R.M. Campbell, Histone modifications and Cancer, Cold Spring Harb. Perspect. Biol. 8 (2016) a019521.
[18] L.T. Kagohara, G.L. Stein-O'Brien, D. Kelley, E. Flam, H.C. Wick, L.V. Danilova, H. Easwaran, A.V. Favorov, J. Qian, D.A. Gaykalova, E.J. Fertig, Epigenetic regulation of gene expression in cancer: techniques, resources and analysis, Brief. Funct. Genomics 17 (2018) 49–63.
[19] M.E. Neganova, S.G. Klochkov, Y.R. Aleksandrova, G. Aliev, Histone modifications in epigenetic regulation of cancer: perspectives and achieved progress, Semin. Cancer Biol. 83 (2022) 452–471.
[20] C. Chen, J. Liu, Histone acetylation modifications: a potential targets for the diagnosis and treatment of papillary thyroid cancer, Front. Oncol. 12 (2022) 1053618.
[21] T.F. Chen, H.F. Hao, Y. Zhang, X.Y. Chen, H.S. Zhao, R. Yang, P. Li, L.X. Qiu, Y. H. Sang, C. Xu, S.X. Liu, HBO1 induces histone acetylation and is important for non-small cell lung cancer cell growth, Int. J. Biol. Sci. 18 (2022) 3313–3323.
[22] G. Xu, L. Niu, Y. Wang, G. Yang, X. Zhu, Y. Yao, G. Zhao, S. Wang, H. Li, HDAC6-dependent deacetylation of TAK1 enhances sIL-6R release to promote macrophage M2 polarization in colon cancer, Cell Death Dis. 13 (2022) 888.
[23] T. Wang, Z. Lu, T. Han, Y. Wang, M. Gan, J.B. Wang, Deacetylation of Glutaminase by HDAC4 contributes to lung Cancer tumorigenesis, Int. J. Biol. Sci. 18 (2022) 4452–4465.
[24] D. Zhang, Z. Tang, H. Huang, G. Zhou, C. Cui, Y. Weng, W. Liu, S. Kim, S. Lee, M. Perez-Neut, J. Ding, D. Czyz, R. Hu, Z. Ye, M. He, Y.G. Zheng, H.A. Shuman, L. Dai, B. Ren, R.G. Roeder, L. Becker, Y. Zhao, Metabolic regulation of gene expression by histone lactylation, Nature 574 (2019) 575–580.
[25] M. Fan, K. Yang, X. Wang, L. Chen, P.S. Gill, T. Ha, L. Liu, N.H. Lewis, D. L. Williams, C. Li, Lactate promotes endothelial-to-mesenchymal transition via Snail1 lactylation after myocardial infarction, Sci. Adv. 9 (2023) eadc9465.

[26] J. Yu, P. Chai, M. Xie, S. Ge, J. Ruan, X. Fan, R. Jia, Histone lactylation drives oncogenesis by facilitating m(6)a reader protein YTHDF2 expression in ocular melanoma, Genome Biol. 22 (2021) 85.
[27] C. Moreno-Yruela, D. Zhang, W. Wei, M. Bæk, W. Liu, J. Gao, D. Danková, A. L. Nielsen, J.E. Bolding, L. Yang, S.T. Jameson, J. Wong, C.A. Olsen, Y. Zhao, Class I histone deacetylases (HDAC1-3) are histone lysine delactylases, Sci. Adv. 8 (2022) eabi6696.
[28] K. Tomczak, P. Czerwińska, M. Wiznerowicz, The Cancer genome atlas (TCGA): an immeasurable source of knowledge, Contemporary oncology (Poznan, Poland) 19 (2015) A68–A77.
[29] Z. Tang, B. Kang, C. Li, T. Chen, Z. Zhang, GEPIA2: an enhanced web server for large-scale expression profiling and interactive analysis, Nucleic Acids Res. 47 (2019) W556–w560.
[30] Giorgi, F. M., Ceraolo, C., and Mercatelli, D. (2022) The R Language: An Engine for Bioinformatics and Data Science. Life (Basel, Switzerland) (12).
[31] J.A. Castro-Mondragon, R. Riudavets-Puig, I. Rauluseviciute, R.B. Lemma, L. Turchi, R. Blanc-Mathieu, J. Lucas, P. Boddie, A. Khan, N. Manosalva Pérez, O. Fornes, T.Y. Leung, A. Aguirre, F. Hammal, D. Schmelter, D. Baranasic, B. Ballester, A. Sandelin, B. Lenhard, K. Vandepoele, W.W. Wasserman, F. Parcy, A. Mathelier, JASPAR 2022: the 9th release of the open-access database of transcription factor binding profiles, Nucleic Acids Res. 50 (2022) D165–d173.
[32] National Research Council Committee for the Update of the Guide for the, C., and Use of Laboratory, A. (2011) The National Academies Collection: Reports funded by National Institutes of Health. In *Guide for the Care and Use of Laboratory Animals*, National Academies Press (US) Copyright © 2011, National Academy of Sciences., Washington (DC).
[33] S. Brabletz, H. Schuhwerk, T. Brabletz, M.P. Stemmler, Dynamic EMT: a multi-tool for tumor progression, EMBO J. 40 (2021) e108647.
[34] B. Bakir, A.M. Chiarella, J.R. Pitarresi, A.K. Rustgi, EMT, MET, plasticity, and tumor metastasis, Trends Cell Biol. 30 (2020) 764–776.
[35] T. Hell, M. Dobrzyński, F. Gröflin, J.K. Reinhardt, L. Dürr, O. Pertz, M. Hamburger, E. Garo, Flavonoids from Ericameria nauseosa inhibiting PI3K/AKT pathway in human melanoma cells, Biomed. Pharmacother. 156 (2022) 113754.
[36] A. Glaviano, A.S.C. Foo, H.Y. Lam, K.C.H. Yap, W. Jacot, R.H. Jones, H. Eng, M. G. Nair, P. Makvandi, B. Geoerger, M.H. Kulke, R.D. Baird, J.S. Prabhu, D. Carbone, C. Pecoraro, D.B.L. Teh, G. Sethi, V. Cavalieri, K.H. Lin, N.R. Javidi-Sharifi, E. Toska, M.S. Davids, J.R. Brown, P. Diana, J. Stebbing, D.A. Fruman, A.P. Kumar, PI3K/AKT/mTOR signaling transduction pathway and targeted therapies in cancer, Mol. Cancer 22 (2023) 138.
[37] M. Song, Q. Pan, J. Yang, J. He, J. Zeng, S. Cheng, Y. Huang, Z.Q. Zhou, Q. Zhu, C. Yang, Y. Han, Y. Tang, H. Chen, D.S. Weng, J.C. Xia, Galectin-3 favours tumour metastasis via the activation of β-catenin signalling in hepatocellular carcinoma, Br. J. Cancer 123 (2020) 1521–1534.
[38] H. Luo, J. Chang, Y. Ren, X. Zhang, Y. Li, M. Huo, H. Wang, X. Yang, J. Liu, Q. Zhang, Y. Zhao, W. Wang, Inhibition of ITGA2 suppresses cervical tumorigenesis and metastasis by targeting the AKT/mTOR signaling pathway, Genes & diseases 12 (2025) 101328.
[39] Y. Hu, Y. Zheng, M. Dai, J. Wu, B. Yu, H. Zhang, W. Kong, H. Wu, X. Yu, Snail2 induced E-cadherin suppression and metastasis in lung carcinoma facilitated by G9a and HDACs, Cell Adh. Migr. 13 (2019) 285–292.
[40] M.Z. Wu, Y.P. Tsai, M.H. Yang, C.H. Huang, S.Y. Chang, C.C. Chang, S.C. Teng, K. J. Wu, Interplay between HDAC3 and WDR5 is essential for hypoxia-induced epithelial-mesenchymal transition, Mol. Cell 43 (2011) 811–822.
[41] Li, C. H., Liang, S. B., Huang, Q. W., Zhou, Z. Z., Ding, Z., Long, N., Wi, K. C., Li, L., Jiang, X. P., Fan, Y. J., and Xu, Y. Z. (2024) Minor Spliceosomal 65K/RNPC3 Interacts with ANKRD11 and Mediates HDAC3-Regulated Histone Deacetylation and Transcription. *Advanced Science* (Weinheim, Baden-Wurttemberg, Germany), (e2307804).
[42] J. Tímár, A. Ladányi, Metastatic progression of human melanoma, Cancers 15 (2023).
[43] T. Tan, P. Shi, M.N. Abbas, Y. Wang, J. Xu, Y. Chen, H. Cui, Epigenetic modification regulates tumor progression and metastasis through EMT (review), Int. J. Oncol. 60 (2022).
[44] M.G. Davey, N. Miller, N.M. McInerney, A review of epidemiology and Cancer biology of malignant melanoma, Cureus 13 (2021) e15087.
[45] N. Turner, O. Ware, M. Bosenberg, Genetics of metastasis: melanoma and other cancers, Clin. Exp. Metastasis 35 (2018) 379–391.
[46] M. Arnold, D. Singh, M. Laversanne, J. Vignat, S. Vaccarella, F. Meheus, A.E. Cust, E. de Vries, D.C. Whiteman, F. Bray, Global burden of cutaneous melanoma in 2020 and projections to 2040, JAMA Dermatol. 158 (2022) 495–503.
[47] P. Horak, K. Kreisingerova, J. Reda, L. Ondrusova, J. Balko, J. Vachtenheim Jr., P. Zakova, J. Vachtenheim, The hedgehog/GLI signaling pathway activates transcription of slug (Snail2) in melanoma cells, Oncol. Rep. 49 (2023).
[48] J.H. Wang, L. Mao, J. Wang, X. Zhang, M. Wu, Q. Wen, S.C. Yu, Beyond metabolic waste: lysine lactylation and its potential roles in cancer progression and cell fate determination, Cell. Oncol. (Dordr.) 46 (2023) 465–480.
[49] Q. Fu, A. Cat, Y.G. Zheng, New histone lysine acylation biomarkers and their roles in epigenetic regulation, Current protocols 3 (2023) e746.
[50] Y. Xie, H. Hu, M. Liu, T. Zhou, X. Cheng, W. Huang, L. Cao, The role and mechanism of histone lactylation in health and diseases, Front. Genet. 13 (2022) 949252.
[51] H. Xu, L. Li, S. Wang, Z. Wang, L. Qu, C. Wang, K. Xu, Royal jelly acid suppresses hepatocellular carcinoma tumorigenicity by inhibiting H3 histone lactylation at H3K9la and H3K14la sites, Phytomedicine : international journal of phytotherapy and phytopharmacology 118 (2023) 154940.
[52] J. Yang, L. Luo, C. Zhao, X. Li, Z. Wang, Z. Zeng, X. Yang, X. Zheng, H. Jie, L. Kang, S. Li, S. Liu, C. Zhou, H. Liu, A positive feedback loop between inactive VHL-triggered histone Lactylation and PDGFRβ signaling drives clear cell renal cell carcinoma progression, Int. J. Biol. Sci. 18 (2022) 3470–3483.
[53] H. Fan, F. Yang, Z. Xiao, H. Luo, H. Chen, Z. Chen, Q. Liu, Y. Xiao, Lactylation: novel epigenetic regulatory and therapeutic opportunities. *American journal of physiology*, Endocrinol. Metab. 324 (2023) E330–e338.
[54] J. Jin, L. Bai, D. Wang, W. Ding, Z. Cao, P. Yan, Y. Li, L. Xi, Y. Wang, X. Zheng, H. Wei, C. Ding, Y. Wang, SIRT3-dependent delactylation of cyclin E2 prevents hepatocellular carcinoma growth, EMBO Rep. 24 (2023) e56052.